Supporting Information

Perfluoropentane-filled chitosan poly-acrylic acid nanobubbles with high stability for long-term ultrasound imaging in vivo

Xuemei Gao, Dajing Guo, Xiang Mao, Xuefeng Shan, Xuemei He, Chaoqun Yu*

Study of the re-dispersion of PFP-CS-PAA nanobubbles by cold water.

The PFP-CS-PAA nanobubbles were re-dispersed by cold water below 29 ˚C, and then the suspension (7 mg/mL) were poured into latex glove and imaged in a tank filled with degassed and deionized water at 37 ˚C. The samples were scanned using an ultrasonic diagnostic instrument (Mylab90; Esaote SpA, Genova, Italy) in both conventional B mode and non-linear harmonic imaging mode. The ultrasound mechanical index (MI) was changed from 0.05 to 0.3 and the frequency of the transducer was 7 MHz. As it was showed in figure S1, after being re-dispersed by cold water below 29 ˚C, the re-dispersed nanobubbles showed very poor imaging capability. The reason was that the PFP is in liquid-form below 29 ˚C and can change into gas-form above 29 ˚C. If the PFP-CS-PAA nanobubbles were re-dispersed in cold water below 29˚C, the vaporized PFP in nanobubbles would change into liquid-form again and then negative pressure formed in the hollow space of nanobubbles. The negative pressure in nanobubbles might make nanobubbles shrink or make water outside of the nanobubbles being sucked into the internal hollow space. As a result, PFP-CS-PAA nanobubbles would significantly lose its imaging capability if the nanobubbles were re-dispersed by cold water below 29 ˚C.

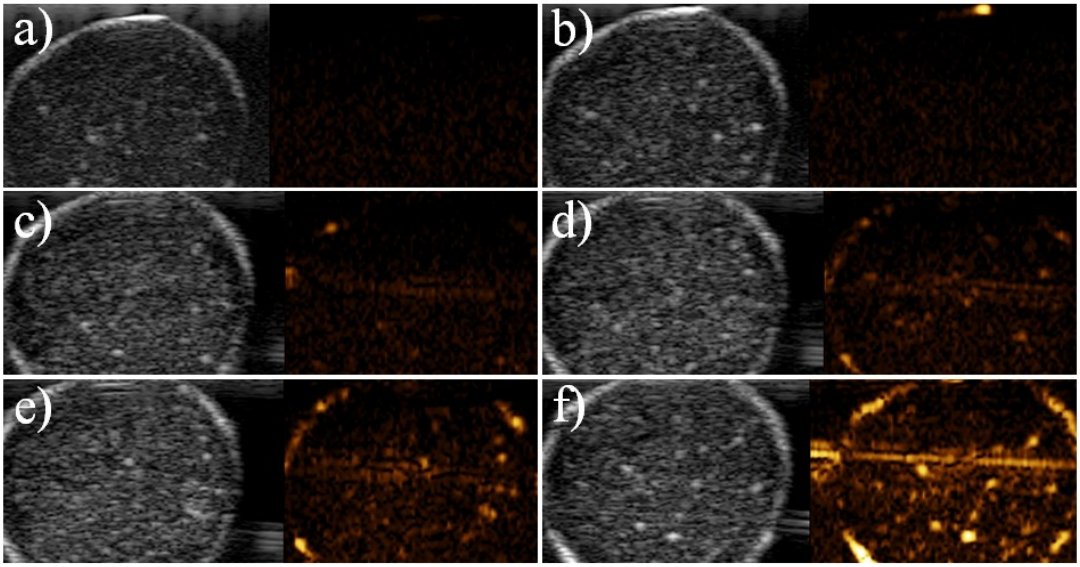

Figure S1. Typical B-mode and non-linear harmonic mode ultrasound images of the PFP-CS-PAA nanobubbles re-dispersed by cold water below 29 ˚C at different mechanical index, (a) 0.05, (b) 0.10, (c) 0.15, (d) 0.20, (e) 0.25, (f) 0.30.

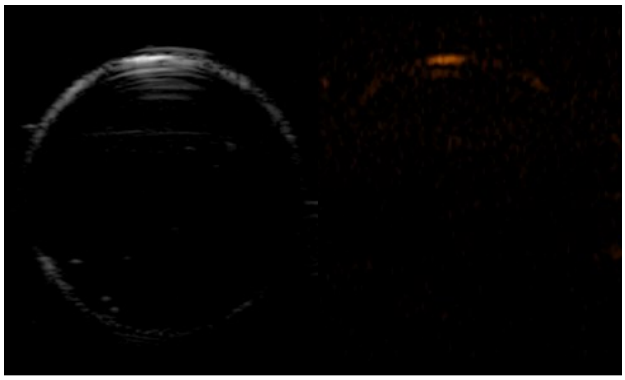

Figure S2. Typical ultrasound image of the CS-PAA hollow nanoparticle suspension in vitro.

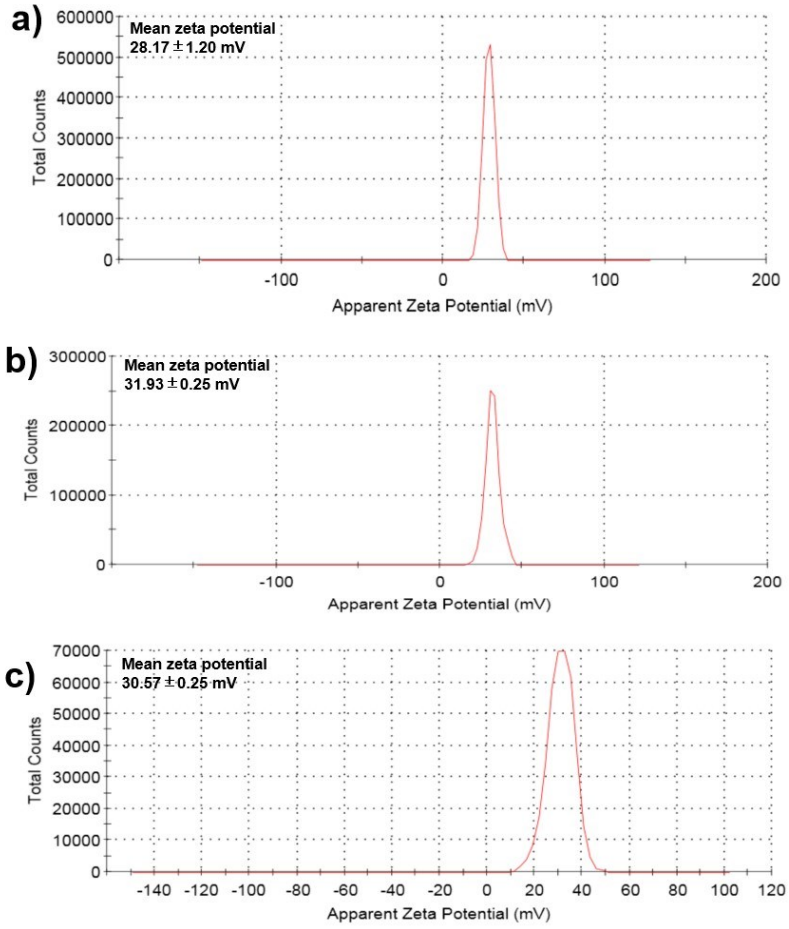

Figure S3. Typical zeta potential graphs of the CS-PAA hollow nanoparticle suspension (a), the re-dispersed lyophilized CS-PAA hollow nanoparticles (b) and the PFP-CS-PAA nanobubbles (c).

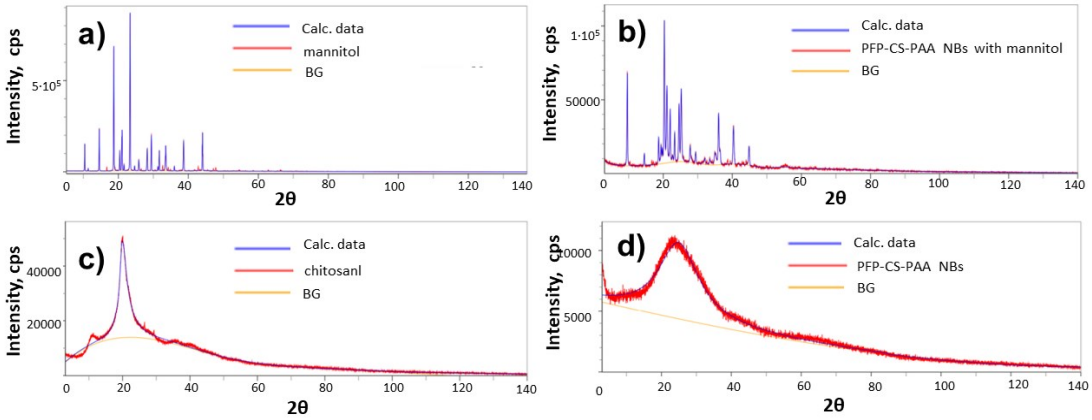

Figure S4. XRD spectra of mannitol (a), PFP-CS-PAA NBs with mannitol (b), chitosan (c), and PFP-CS-PAA NBs without mannitol (d).

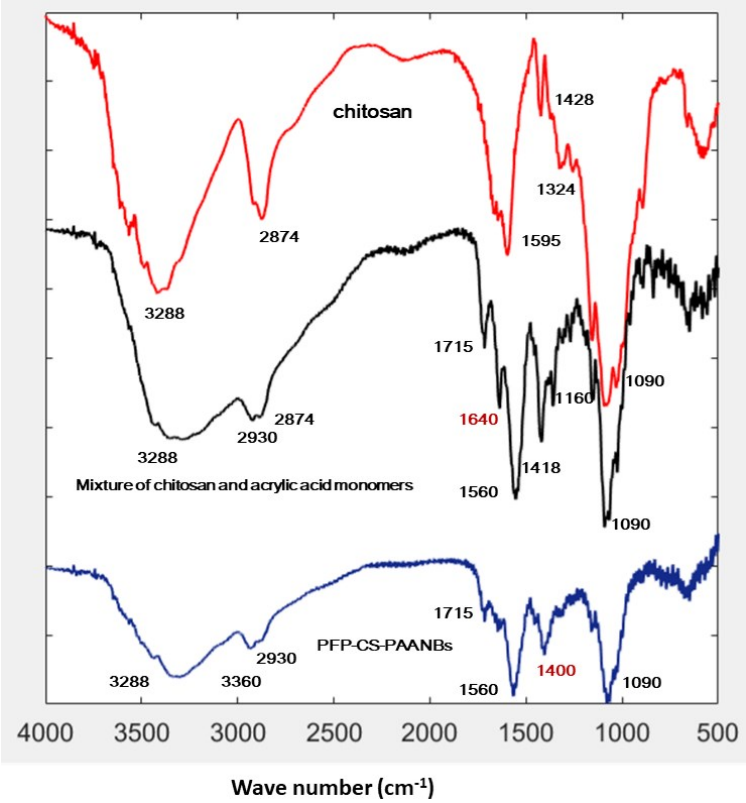

Figure S5. FT-IR spectra of chitiosan, mixture of chitosan and acrylic acid monomers and PFP-CS-PAA NBs

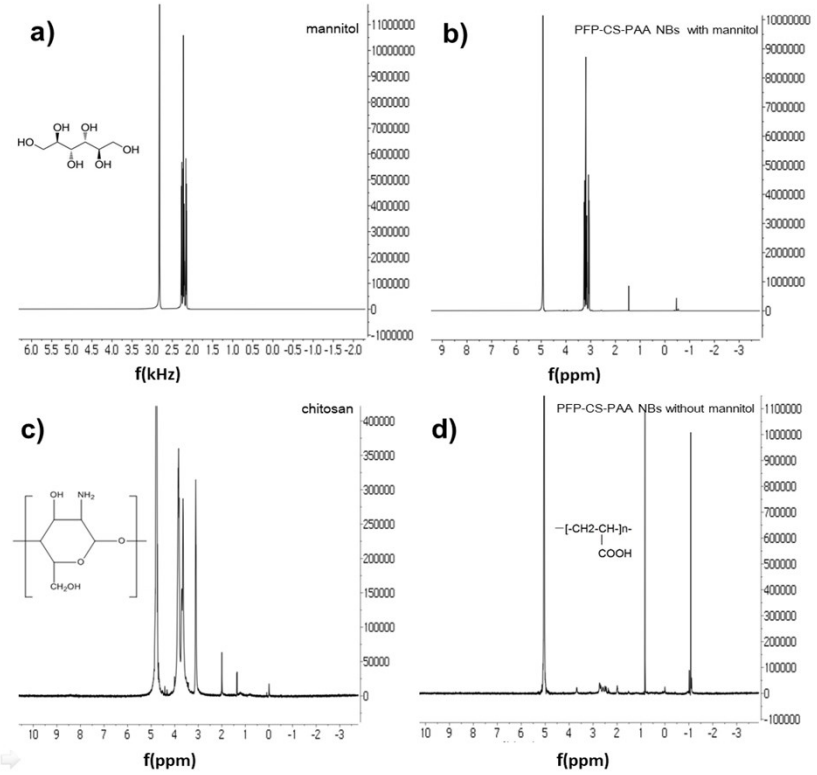

Figure S6. ^{1}H NMR spectrum of mannitol (a), PFP-CS-PAA NBs with mannitol (b), chitosan (c), and PFP-CS-PAA NBs without mannitol (d).

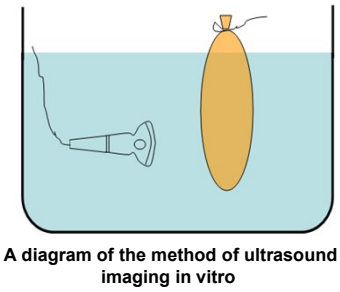

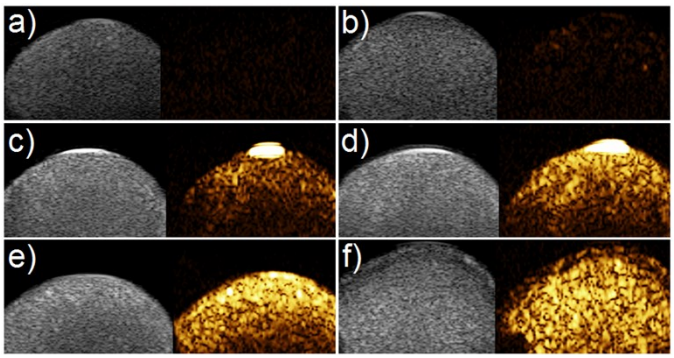

Figure S7 Typical in vitro B-mode and non-linear harmonic mode ultrasound images of the PFP-CS-PAA nanobubbles at different mechanical indexs (MIs), (a) 0.05, (b) 0.10, (c) 0.15, (d) 0.20, (e) 0.25, (f) 0.30;

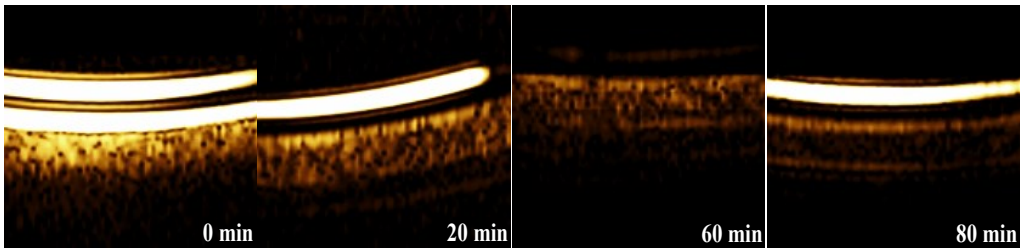

Figure S8. Typical ultrasound images of the longitudinal cross-section of silicone tube within PFP-CS-PAA nanobubbles suspension at different times under flow state.

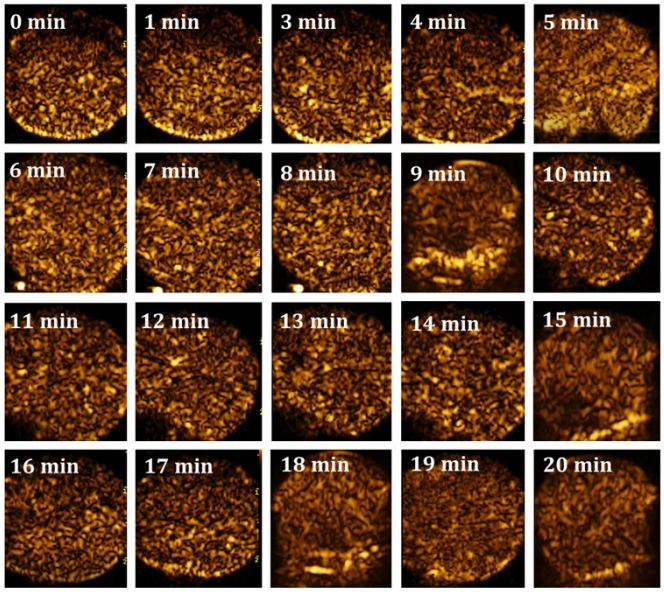

Figure S9. Typical ultrasound images of the PFP-CS-PAA NBs under continous ultrasonic irradiation within 20 min.

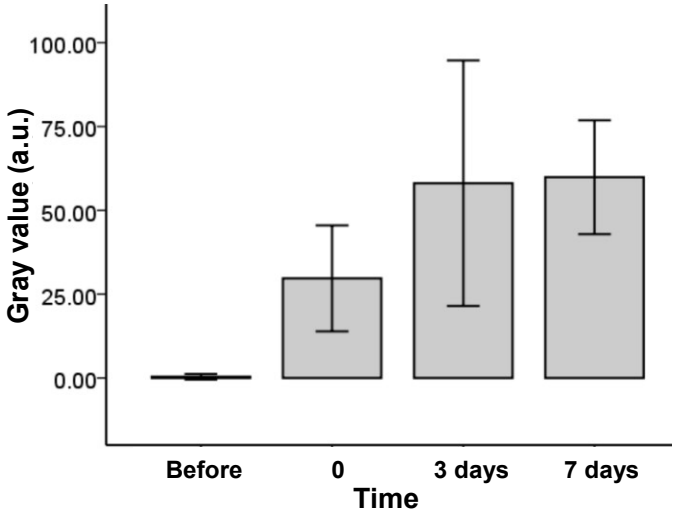

Figure S10 Gray values of harmonic mode ultrasound images of the PFP-CS-PAA nanobubbles before intra-tumoral injection, after intra-tumoral injection immediately, after intra-tumoral injection for 3 days and 7 days (n=3).

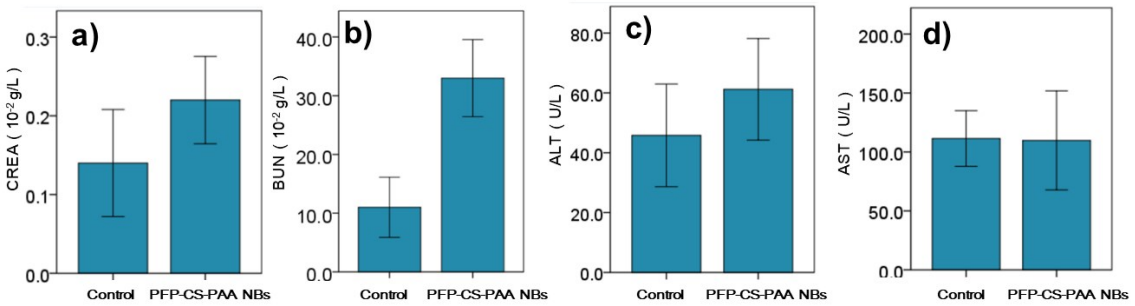

Figure S11. The liver functional markers (ALT and AST) and kidney functional markers (CREA and BUN) of the control and PFP-CS-PAA NBs groups after intravenous injection (n=5).

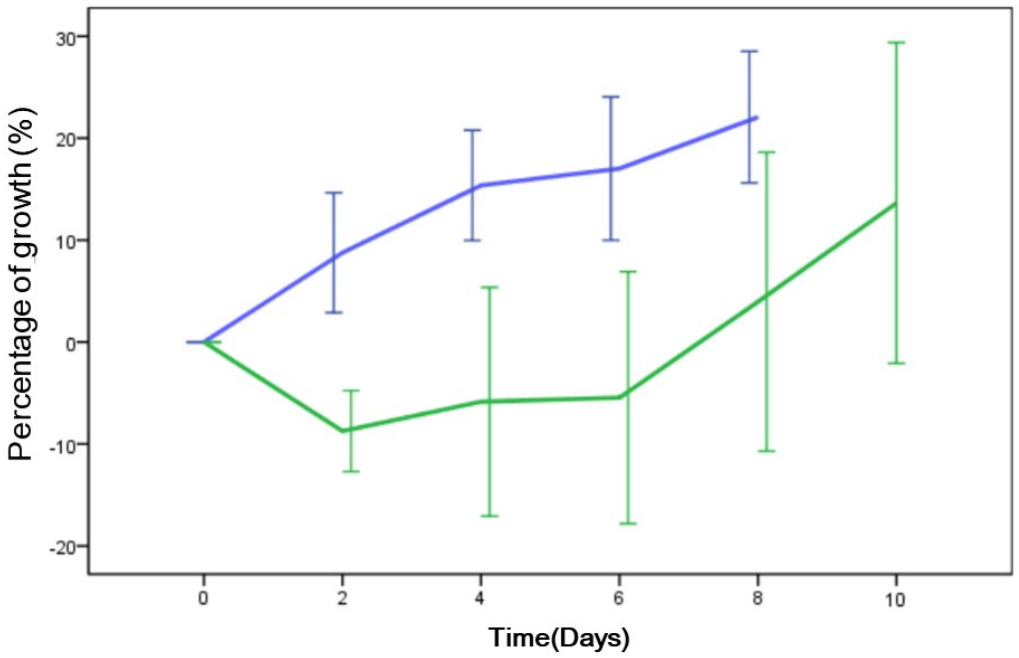

Figure S12. The weight change of SD rats of the control and PFP-CS-PAA NBs groups after intravenous injection (n=5).